



ELSEVIER

Available online at [www.sciencedirect.com](http://www.sciencedirect.com)

SCIENCE @ DIRECT®

Journal of Magnetism and Magnetic Materials 286 (2005) 473–478



[www.elsevier.com/locate/jmmm](http://www.elsevier.com/locate/jmmm)

# Spin-resolved magnetic studies of BCT Fe/Mn/BCT Fe(1 0 0)/FCC Pd(1 0 0) films using scanning ion microscopy with polarization analysis

Jian Li, Carl Rau\*

*Department of Physics and Astronomy, Rice Quantum Institute and Center for Nanoscience and Technology, Rice University, Houston, TX 77251, USA*

Available online 12 October 2004

## Abstract

We report on spin-resolved magnetic studies of wedge-shaped, epitaxial BCT Fe/Mn/BCT Fe(1 0 0)/FCC Pd(1 0 0) films by using scanning ion microscopy with polarization analysis (SIMPA) and magneto-optical Kerr effect (MOKE). SIMPA is used to perform in situ spin-resolved magnetic domain imaging, and MOKE is utilized to study magnetic hysteresis loops. Fe/Mn/Fe films are deposited on well-prepared, atomically flat Pd(1 0 0) substrates. Medium energy electron diffraction (MEED) and Auger electron spectroscopy (AES) are used for detailed studies of growth modes, surface and interface structures. Various non-uniform, curling domain and domain wall structures, which are strongly affected by canted magnetic couplings, are found.

© 2004 Elsevier B.V. All rights reserved.

PACS: 75.60.Ch; 75.70Rf; 68.65.Ac; 71.70.Gm; 75.25.+z

Keywords: Domain structure; Domain imaging; Magnetic coupling; Fe; Mn; Pd; SIMPA; Spin polarization; Spin map

Magnetic phenomena such as magnetic couplings (MC) between two ferromagnetic layers through a magnetic or non-magnetic spacer layer receive great attention [1–9]. The system Fe/Mn/Fe is very interesting, because Mn shows anti-ferromagnetic ordering in the bulk. The MC

between magnetic layers, separated by a spacer layer, often oscillates periodically from ferromagnetic (FM) to antiferromagnetic (AF) as function of the thickness of the spacer layer. In addition, there exist 90°, canted and other forms of non-collinear MC. For non-magnetic metallic spacer layers, MC can be characterized by the following Heisenberg-type, phenomenological energy series [1]  $E_c = -J_1 \cos(\theta) - J_2 \cos^2(\theta) + \dots$ , where  $\theta$  is the angle between the magnetization vectors of the

\*Corresponding author. Tel.: +1 713 348 5417; fax: +1 713 348 4150.

E-mail address: [rau@rice.edu](mailto:rau@rice.edu) (C. Rau).

two FM layers,  $J_1$  represents the bilinear coupling, which aligns the magnetic moments parallel for  $J_1 > 0$  and antiparallel for  $J_1 < 0$ , and  $J_2$  describes  $90^\circ$  (biquadratic) MC, which creates a perpendicular alignment of the magnetic moments for  $J_2 < 0$ . However, if the spacer layer is AF, the MC between the AF spacer material and the FM layers, as well as the MC within the AF spacer layer must be considered [1–9]. Slonczewski [1] proposed a proximity magnetism model, which is a phenomenological model for the description of MC across AF spacer layers and also includes effects of thickness fluctuations on details of the MC. The MC is expressed by a non-Heisenberg-type coupling formula  $E_c = C_+ \theta^2 + C_- (\theta - \pi)^2$ , where  $C_+$  and  $C_-$  are coupling coefficients, which can be positive or zero. If  $C_+$  and  $C_-$  are non-zero, then the MC is non-collinear, if either  $C_-$  or  $C_+$  is zero, then the MC is collinear (FM or AF), for  $C_+ = C_-$ ,  $90^\circ$  MC is obtained.

Purcell et al. [2] find for BCC Fe(100)/Mn/BCC Fe(100) films AF MC with two monolayer (ML) oscillation periods for 4–7 MLs of Mn. Filipkowski et al. [3] report on the existence of near- $90^\circ$  MC in BCC CoFe(100)/Mn/BCC CoFe(100) sandwich structures grown on GaAs(100) with no evidence for  $180^\circ$  MC. Yan et al. [4–6] studied BCC Fe/Mn/BCC Fe trilayers grown on a GaAs/Fe/Ag substrate–buffer system and find that the angle between the magnetization vectors of the two magnetic Fe(100) layers increases gradually from  $0^\circ$  to about  $180^\circ$  and then gradually reduces to  $90^\circ$  for Mn thicknesses from 0.62 to 1.2 nm. For Mn layer thicknesses in the range between 1.2 and 2.45 nm, the MC is always  $90^\circ$ , with its strength oscillating with a short period of about 2 ML. Tulchinsky et al. [7] and Pierce et al. [8] utilized scanning electron microscopy with polarization analysis (SEMPA) to measure magnetic domain distributions of wedge-shaped BCC Fe/Mn/BCC Fe(001) trilayers. They find non-collinear, canted MC. Similarly, Yan et al. [6] employed Kerr microscopy to study magnetic domain structures of BCC Fe/Mn/BCC Fe(001) films and find evidence for non-collinear MC between the Fe films. To the best of our knowledge, there are no experimental studies on MC for BCC Fe(100) films with Mn as spacer layers.

In this paper, using scanning ion microscopy with polarization analysis (SIMPA) [10,11], we report on detailed studies of the spatially- and spin-resolved magnitude and orientation of the magnetization of domain and domain wall structures of well-characterized, wedged BCT Fe/Mn/BCT Fe films deposited pseudomorphically on surfaces of highly oriented, atomically flat Pd(100) substrate crystals as function of Mn spacer layer thickness. It is found that the MC strongly affects locally the detailed magnetic structure within the magnetic domains and domain walls of the top BCT Fe(100) films.

For the deposition of wedged Fe/Mn/Fe films, atomically clean and flat FCC Pd(100)p(1 × 1) surfaces are prepared in ultra-high vacuum (UHV) in a target preparation chamber operating at  $2 \times 10^{-10}$  mbar [12–15]. The surface orientation of the crystals is better than  $0.01^\circ$ , and is monitored by using a precision X-ray diffractometer. Applying standard cleaning and annealing procedures, developed in earlier studies [14,15], and using Auger electron spectroscopy (AES), residual C and O contaminations are less than 1% of a ML. Using electron beam evaporation for the deposition of Fe films, a substrate temperature of 293 K and an evaporation rate of 0.002 nm/s, island-free, homogeneous, pseudomorphic, layer-by-layer growth is detected by quantitative AES and medium energy electron diffraction (MEED) up to 50 MLs of BCT Fe(100)p(1 × 1) [12–19]. MEED studies show that the  $\langle 100 \rangle$  axes of BCT Fe(100) are oriented parallel to the  $\langle 110 \rangle$  axes of FCC Pd(100). Subsequently, using a movable shutter, 1–9 ML of Mn are deposited by thermal evaporation at  $4 \times 10^{-10}$  mbar with an evaporation rate of 0.001 nm/s. Excellent pseudomorphic, layer-by-layer growth of the Mn films is found for a substrate temperature of 293 K as detected by MEED oscillations and quantitative AES. Note there is no interdiffusion at the Fe/Pd interfaces for temperatures below  $300^\circ\text{C}$  and for Mn/Fe interfaces below  $200^\circ\text{C}$  [18]. Quinn et al. [19] find that FCT Mn grows pseudomorphically on FCC Pd(100), which provides the same square lattice mesh as BCT Fe/FCC Pd(100). Therefore, for good epitaxy, as found for 1–9 ML of Mn, a FCT structure of the Mn films is anticipated [18].

Following the deposition of the Mn wedge, 35 ML of BCT Fe(100) are evaporated on top of the Mn wedge. Finally, the topmost Fe layer is covered with a 0.5 nm thick Au film to prevent contamination of the sample during transfer from the preparation chamber to the Magneto-optical Kerr effect (MOKE)/SIMPA chambers [10,11,18], where they are studied under UHV conditions by using MOKE and SIMPA.

From MOKE experiments, it is found that, for all Mn spacer layer thicknesses studied so far, four-fold magnetic anisotropies exist along the easy axis directions of the films, which are oriented along the  $\langle 100 \rangle$  directions of the BCT Fe(100)/Mn/BCT Fe(100) films, which are oriented along the  $\langle 110 \rangle$  directions of Pd(100). No uniaxial magnetic anisotropies, which could be induced by different growth modes [16,17] are found.

Subsequently, the samples are transferred in situ from the MOKE chamber to the SIMPA microscope, which is located in an UHV chamber operating at  $2 \times 10^{-10}$  mbar. This chamber houses a scanning, microfocused (minimum spot size: 35 nm), 6–30 keV  $\text{Ga}^+$  ion beam facility, which is used to scan magnetic and non-magnetic surfaces to induce the emission of electrons from the sample surface. By using a Mott detector, the orientation and magnitude of the local spin polarization  $P$  of the emitted electrons is analyzed in order to obtain spin-resolved images of magnetic domains and domain walls [10,11]. The SIMPA technique offers some unique advantages compared to many other magnetic imaging techniques, because of its capability to produce vectorial maps of the surface magnetization by directly measuring the spatially resolved vector orientation and magnitude of  $P$ , which is a characteristic of the surface magnetization [10,11]. Before the SIMPA measurements, the Au film is sputtered off, and the samples are demagnetized to reduce magnetostatic effects.

Fig. 1 is obtained by using SIMPA at the surface of BCT Fe (35 ML)/Mn/BCT Fe(50 ML)/Pd(100) films for a Mn layer thickness  $d_{\text{Mn}} \leq 1$  ML. The SIMPA spin map consists of three differently oriented magnetic domains with the local distribution of the in plane orientation and magnitude of the  $P$  vectors given by white arrows. The different

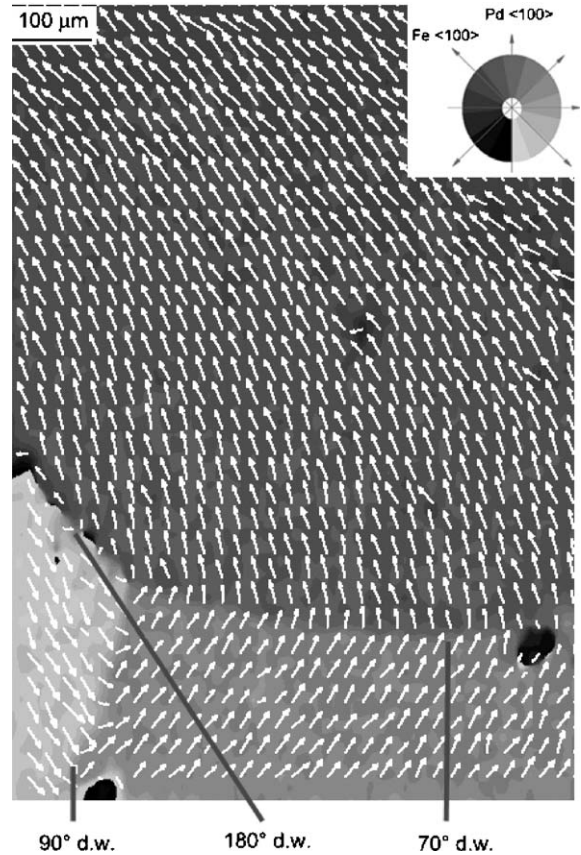


Fig. 1. SIMPA spin map of the surface of a BCT Fe(35 ML)/Mn/BCT Fe(50 ML) film for a Mn layer thickness  $d_{\text{Mn}} \leq 1$  ML. The local distribution of the orientation and magnitude of the  $P$  vectors is shown by white arrows. (domain wall: d.w.).

gray shades in the image represent different orientations of the in plane polarization  $P$  as given by the gray shade wheel in the upper right part of Fig. 1, which also gives the directions of the  $\langle 100 \rangle$  directions of BCT Fe(100) and FCC Pd(100) and allows a simple identification of magnetic domains and walls. In order to obtain a clear plot of the  $P$  vectors and to account for statistical fluctuations in electron count rates,  $P$  is first averaged over four nearest neighbors, and then only every 16th  $P$  vector is plotted, thereby reducing the density of  $P$  vectors by a factor of 64. Clearly visible are an  $180^\circ$  domain wall, a  $90^\circ$  domain wall and a  $70^\circ$  domain wall. Note that local  $P$  vectors are strongly changing within the

domain walls, and that  $P$  is gradually changing (curling) within the magnetic domains towards one of the  $\langle 100 \rangle$  easy directions of magnetization of BCT Fe(100). Without MC, the  $P$  vectors in the domains should be aligned along one of these easy axes. It is obvious that the competition between magnetocrystalline anisotropy and canted MC [7,8] causes the  $70^\circ$  angle between the  $P$  vectors at the  $70^\circ$  domain wall, which is obtained from line scans. This angle gradually increases to  $90^\circ$ , becoming aligned along an  $\langle 100 \rangle$  easy axis of BCT Fe(100). Using the formula from the proximity magnetism model proposed by Slonczewski [1] and discussed in the introduction, we obtain from our SIMPA measurement, for a canting angle of  $70^\circ$ , a value of 1.52 for the ratio  $C_+/C_-$  of the coupling constants.

Fig. 2a shows a SIMPA spin map, with the same resolution as Fig. 1, obtained at surfaces of BCT Fe(35 ML)/Mn/BCT Fe(50 ML)/Pd(100) wedged films for  $d_{\text{Mn}} = 3$  ML. As for Fig. 1, the density of plotted  $P$  vectors is reduced by a factor of 64, and a gray shade wheel is given in the lower right part of Fig. 2a. The overall size of the domains is reduced and domain walls with angles near and at

$90^\circ$  become more dominant compared to those with an angle of  $180^\circ$ . Compared to Fig. 1, the curling of the  $P$  vectors in the domains is stronger, more non-uniform and show less tendency to be aligned along one of the easy axes of BCT Fe(100).

Fig. 2b gives an enlarged spin map of the area marked in Fig. 2a showing many cross-tie-like magnetic patterns with circular and cross-Bloch lines [20], making the distinction between domains and domain walls less pronounced and indicating, from the reduced magnitude of the  $P$  vectors near and at the center of the circular and cross-Bloch lines, the existence of non-zero, perpendicular  $P$  components pointing out of the surface plane. For easy identification of the cross-tie like magnetic patterns, in Fig. 2c an enlarged spin map of the area marked in Fig. 2b is presented, showing one cross-tie-like pattern with 1 cross and 2 circular Bloch lines, which obviously results from the collapse of a  $180^\circ$  magnetic domain wall. To this we note, that from line scans across all domain walls visible in Figs. 2b and c, we can exclude the existence of  $45^\circ$  domain walls, which one would expect to be found after collapse of  $180^\circ$  degree

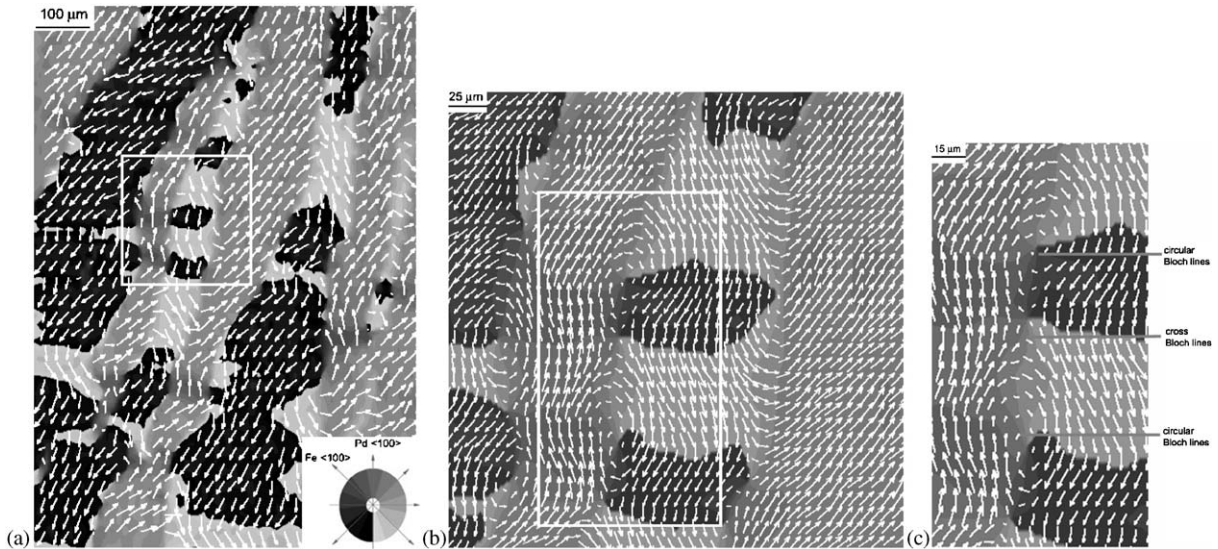


Fig. 2. (a) SIMPA spin map of the surface of a BCT Fe(35 ML)/Mn/BCT Fe(50 ML) film for  $d_{\text{Mn}} = 3$  ML. (b) Enlarged SIMPA image of the area marked in Fig. 2 (a) depicting many cross-tie-like magnetic patterns with circular and cross-Bloch lines. (c) Enlarged SIMPA spin map of the area marked in (b) showing one cross-tie like magnetic pattern, where one cross and two circular Bloch lines are marked.



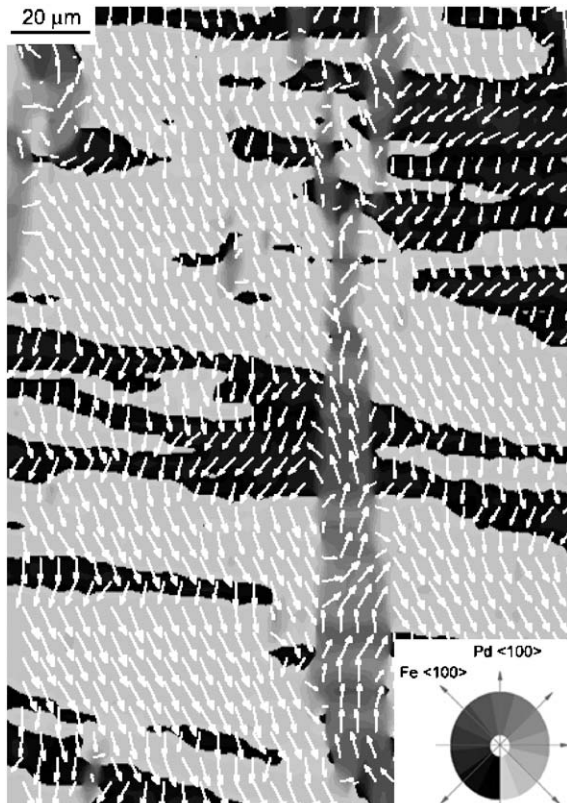


Fig. 3. SIMPA spin map of the surface of a BCT Fe(35 ML)/Mn/BCT Fe(50 ML) film for  $d_{\text{Mn}} = 7$  ML.

domain walls. All line scans show a predominance of domain walls with angles at and close to  $70^\circ$ .

Fig. 3 shows a SIMPA spin map of a BCT Fe(35 ML)/Mn/BCT Fe(50 ML)/Pd(100) film for  $d_{\text{Mn}} = 7$  ML. It is evident that no  $180^\circ$  magnetic domain walls are present, and mostly  $70^\circ$  domain walls and cross-tie like magnetic patterns are found, which is also found for 5 and 9 ML thick Mn spacer layers. As for Fig. 1, the density of plotted  $P$  vectors is reduced by a factor of 64 in order to obtain a clear plot of the  $P$  data, however, the resolution for the SIMPA measurement is increased by a factor of 5 compared to that of Figs. 1 and 2a. As in Fig. 1, a gray shade wheel is given in the lower right part of Fig. 3.

In conclusion, we state that the experiments presented here give clear evidence that SIMPA spin mapping is a powerful technique to study

interrelations between magnetic domain structures and MC in magnetic systems. From spin-resolved maps of the surface magnetization of well-prepared and characterized BCT Fe(100)/Mn/BCT Fe(100)/FCC Pd(100) wedged films with Mn spacer film thicknesses between 1 and 9 ML, there is strong evidence that the MC is non-collinear (canted) and strongly influences the surface domain structure of the BCT Fe(100) films for all Mn film thicknesses studied so far. All samples are studied in the demagnetized state, where magnetostatic interactions between the BCT Fe(100) films are greatly reduced. With increasing Mn film thickness  $d_{\text{Mn}}$ ,  $180^\circ$  domain walls are replaced by cross-tie-like magnetic patterns with circular and cross-Bloch lines. With increasing  $d_{\text{Mn}}$ , the surface magnetization becomes more and more non-uniform, as shown by the increasing curling of the locally spin-resolved  $P$  vectors within the magnetic domains, indicating an increase in the canting angles in agreement with the proximity magnetism model [1].

## References

- [1] J.C. Slonczewski, *J. Magn. Magn. Mater.* 150 (1995) 13.
- [2] S.T. Purcell, et al., *Phys. Rev. B* 45 (1992) 13064.
- [3] M.E. Filipkowski, J.J. Krebs, G.A. Prinz, C.J. Gutterrez, *Phys. Rev. Lett.* 75 (1995) 1847.
- [4] Shi-shen Yan, R. Schreiber, F. Voges, C. Osthöver, P. Grünberg, *Phys. Rev. B* 59 (1999) R11641.
- [5] Shi-shen Yan, P. Grünberg, Liang-mo Mei, *J. Appl. Phys.* 88 (2000) 983.
- [6] Shi-shen Yan, P. Grünberg, R. Schäfer, *Phys. Rev. B* 62 (2000) 5765.
- [7] D.A. Tulchinsky, J. Unguris, R.J. Celotta, *J. Magn. Magn. Mater.* 212 (2000) 91.
- [8] D.T. Pierce, A.D. Davies, J.A. Stroschio, D.A. Tulchinsky, J. Unguris, R.J. Celotta, *J. Magn. Magn. Mater.* 222 (2000) 13.
- [9] Eric E. Fullerton, K.T. Riggs, C.H. Sowers, S.D. Bader, A. Berger, *Phys. Rev. Lett.* 75 (1995) 330.
- [10] N.J. Zheng, C. Rau, *Mater. Res. Soc. Symp. Proc.* 313 (1993) 723.
- [11] J. Li, C. Rau, *J. Appl. Phys.* 95 (2004) 6527.
- [12] C. Rau, M. Lu, N. Zheng, in: J.L. Morán-López, J.M. Sanchez (Eds.), *New Trends in Magnetism, Magnetic Materials, and their Applications*, Plenum Press, New York, 1994, p. 195.
- [13] C. Rau, P. Mahavadi, M. Lu, N.J. Zheng, *J. Magn. Magn. Mater.* 148 (1995) 40.
- [14] C. Rau, *Appl. Phys. A* 49 (1989) 579.

- [15] C. Rau, *J. Magn. Magn. Mater.* 30 (1982) 141.
- [16] C. Rau, M. Robert, *IEEE Trans. Magn.* 32 (1996) 4553.
- [17] C. Rau, M. Robert, *Mod. Phys. Lett. B* 10 (1996) 223.
- [18] G. Steierl, Ph.D. Dissertation, Rice University, Houston, 1997, unpublished.
- [19] J. Quinn, Y.S. Li, H. Li, D. Tian, F. Jona, P.M. Marcus, *Phys. Rev. B* 43 (1991) 3959.
- [20] A. Hubert, R. Schäfer, *Magnetic Domains*, Springer, Berlin, 1998.